Deterministic Assembly of 3D Suspended Nanowire Structures

Hongyan Gao[1], Bing Yin[1], Siyu Wu[1], Xiaomeng Liu[1], Tianda Fu[1], Cheng Zhang[2], Jian Lin[2], Jun Yao[1,3,*]

1. Department of Electrical Computer and Engineering, University of Massachusetts, Amherst, MA, USA.
2. Department of Mechanical & Aerospace Engineering, University of Missouri, Columbia, MO, USA.
3. Institute for Applied Life Sciences (IALS), University of Massachusetts, Amherst, MA, USA.

* Corresponding author. Emails: juny@umass.edu (J.Y.)

Abstract

Controlled assembly of nanowire 3D geometry in an addressable way can lead to advanced 3D device integration and application. By combining a deterministic planar nanowire assembly and a transfer process, we show here a versatile method to construct vertically protruding and suspending nanowire structures. The method harnesses the merits from both processes to yield positional and geometric control in individual nanowires. Multiple transfers can further lead to hierarchical multiwire 3D structures. Assembled 3D nanowire structures have well-defined on-substrate terminals that allow scalable addressing and integration. Proof-of-concept nanosenors based on assembled 3D nanowire structures can achieve high sensitivity in force detection.

Key words: nanowire, assembly, 3D structure, nanosensor, pressure sensor, nanoelectronics

Main text

Synthetic nanowires or nanotubes, with well-defined surface topology and geometric symmetry, can yield excellent electronic/optical properties for high-performance nanodevices.[1-3] Over the past decades, the synthetic advances have been accompanied by a great progress in assembly for scaling up device applications.[2-6] The advent of deterministic assembly techniques has raised the potential in transforming thin-film integration into scalable single-element integration.[7-11] A highlight was the construction of a programmable nanowire nanocomputer,[10] in which the nanowire crossbar matrixes were constructed by laying down individual nanowires following circuit design, enabled by a deterministic 'combing' strategy.[9]

The functional merits of synthetic nanowires probably are more prominent in constructing bio-interfaces, in which their nanoscale size, free-standing geometry and mechanical flexibility can be fully exploited for improved spatial resolution, signal sensing and bio-integration.[1,12-14] Such capabilities have led to sensor-innervated cell and tissue interfaces that increasingly blur the boundary between biology and electronics,[15-17] progressing toward the vison of a 'seamless' integration.[18-20] The geometric freedom in nanowires also offers the feasibility in constructing 3D nanowire devices that can further extend the functional advance, leading to improved cell interfaces and signal transductions.[21-23] Nevertheless, these 3D device engineering was still away from the potential of a scalable integration. Recently, the potential was explored by using a revised deterministic 'combing' technique,[24] in which a "U"-shaped recess geometry not only serves as an anchoring point to position nanowire location but also a shape guide to yield nanowire curvature. The entire process was lithography-compatible and lead to a high yield of 3D nanowire probes, although additional steps[21,24] such as interfacial stress engineering and substrate release were involved in order to rotate the curved in-plane nanowires into vertical ones. While a direct assembly of nanowire 3D structures is desirable, previous mechanically guided assembly only applies to membranes with a lateral dimension above micrometer.[25-27] Similar attempt employed to nanowire assembly largely yielded in-plane buckling,[28,29] which is accountable by an increased vertical instability at reduced lateral size.

We propose a strategy for the direct and deterministic assembly of 3D nanowire structures by combining a deterministic assembly of planar nanowires[9,10] and a transfer process.[30] The overall scheme is illustrated in Fig. 1. Briefly, nanowire arrays with defined pitches are assembled by a

deterministic 'combing' technique.[9,10] Assembled nanowire arrays are then coated with a thin polymer layer, which serves as a carrier layer to maintain nanowire position and alignment. The carrier layer, along with attached nanowires, is then peeled off by using a soft stamp and transferred onto a target substrate.[30] Importantly, arrays of microscale bars (microbars), with the pitch sizes matching to those in nanowire arrays, are predefined on the target substrate. Nanowires are perpendicularly aligned to the microbars during the transfer, after which the removal of the carrier layer is expected to leave only suspended nanowires over the microbars. Structural modulation in the microbar can be employed to tune the geometry in nanowire suspension. The nanowire portion extending on the substrate can be used for electrical addressing, enabling 3D device applications.

The prerequisite for above scheme is the deterministic assembly of planar nanowires. We followed a process previously developed[9,10] (Fig. 2a) and used silicon (Si) nanowires with an average diameter of 20 nm for demonstration. Briefly, a thin layer (~50 nm) of photoresist was coated on a Si substrate covered with 600-nm thick surface oxide. Standard photolithography was employed to define narrow windows of open substrate (SiO_2) surface. The freshly exposed SiO_2 surface, functionalized to be hydrophilic by the alkaline component in the developer, becomes highly attractive to Si nanowires.[9,10,31] The resist surface, on the other hand, is hydrophobic and nonattractive to Si nanowires.[9,10] The nanowire growth substrate was then brought to contact the patterned substrate and translated in the direction along the long axis of exposed window. During the process, the protruding end of a nanowire was first captured by the exposed SiO_2 window, with its rest portion being pulled over to the resist surface by shear force for alignment. The hydrophobic resist surface reduces nanowire friction force. Viscous lubricant such as heavy oil was also added between the two substrates to increase the shear force and further reduce friction. Collectively, the alignment force (*i.e.*, shear force subtracting friction force) is maximized to produce effective alignment in nanowires. Careful tuning the window size can lead to the dominancy of single-nanowire anchoring events and hence the deterministic positioning and alignment of individual nanowires.

Fig. 2b shows a representative dark-field image of assembled nanowires in a 10×10 matrix. It shows that nanowires are highly aligned and selectively positioned with well-defined pitch (100 μm). Zoom-in optical image (Fig. 2c) shows that the nanowire is anchored in the exposed SiO_2 window (2×20 μm^2), with the rest portion extended on the resist surface highly aligned (Fig. 2d). Statistics from 900 assembly sites showed that 440 sites (~49%) yielded single-nanowire

anchoring with the extending length ≥10 μm that is preferable for follow-up 3D assembly. 200 cites (~22%) sites were vacant or with nanowire length <10 μm. These values are consistent with previous result obtained in Ge/Si core-shell nanowires with the anchoring windows defined by electron-beam lithography.[10]

The resist layer underneath the nanowires was then removed by oxygen plasma (50 W, 10 min) to yield a direct nanowire-substrate (SiO_2) interface. The strong nanowire-SiO_2 surface interaction allowed subsequent spin-coating of a carrier layer of polymethyl methacrylate (PMMA, 100 nm) without perturbing the nanowire position or alignment. A thin (~1 mm thick) polydimethylsiloxane (PDMS) film was attached onto the PMMA layer as the handle layer during transfer. Water intercalation,[30] which did not introduce any detrimental effect to nanowires, was utilized to peel off the PMMA carrier layer from the SiO_2 substrate (Supplementary Fig. 1). Peeled-off PMMA, attached to the PDMS handle layer, maintained flatness and hence the nanowire position and alignment (Supplementary Fig. 2a). The target substrate was pre-defined with arrays of microbars ($10×0.8×2.1\ \mu m^2$, L×W×H) with the pitch sizes matching to the nanowire arrays. The peeled-off nanowires attached to the PMMA layer was completely dried by nitrogen before transfer process. The optical transparency in the PDMS and PMMA layers allowed aligning the nanowires to the microbars during transfer (Supplementary Fig. 3). An elevated temperature (100 °C for 5 min) thermally released the PDMS layer and left only the PMMA layer on the target substrate. Due to the mechanical flexibility, PMMA layer landed down on both the microbar and the flat region of surface, creating a microscale tent that defined the spanning geometry in the nanowire (Supplementary Fig. 2b). The thermal process also improved the adhesion between the nanowire and SiO_2/microbar surface, for which the subsequent dissolving of the PMMA carrier layer in acetone did not perturb the suspended nanowire structure.

The assembly was examined in a 10×10 matrix covering an area of 1 mm^2 (Fig. 3a), which was only limited by the size of the writing field in electron beam lithography (for defining the microbars). Optical dark-field image of a 5×4 matrix shows the visibility of (transverse) nanowires crossing the (vertical) microbars (Fig. 3b). A zoom-in image indicates the suspending configuration in the nanowire, inferred by a gradual increase in brightness along the nanowire toward the microbar apex (Fig. 3c). The suspension was further confirmed by scanning electron microscopy (SEM) imaging (Fig. 3d), in which nearly symmetric nanowire arms are observed to suspend over the microbars (Fig. 3e). About half of the sites (48/100) yielded nanowire structures

with both arms symmetrically suspended (Fig. 3f), which was consistent to the yield in planar assembly and indicated minimal nanowire breakage during the process. Less sites (18/100) yielded nanowire structures with only one arm suspended, presumably due to insufficient nanowire length that could extend half but not the entire span.

Tuning the heights in the microbars naturally modulated the nanowire protrusions, with the symmetry in the pair of suspended arms maintained (Fig. 3g). The nanowire spanning correspondingly increased with the increase in microbar height from 0.4 to 2.1 µm (Fig. 3h). A trend of gradual increase in the climbing angle (*i.e.*, related to height/spanning ratio) from 22° to 28° was also observed, which was accountable by an energy minimization from the competition between the collapsing forces (*e.g.*, gravity, van der Waals, capillary force) and the internal rigidity in the PMMA layer.[32] Consequently, changing the mechanical property in the carrier layer and/or surface functionality can be expected to modulate the climbing configuration in nanowires. In principle, the nanowire suspension height is not limited with this methodology. Practically, as the local strain experienced in the carrier layer increases with the increase of height in the microbar, the suspension height will be limited by the mechanical robustness in the carrier layer. For example, at a suspension height >4 µm, the average global strain in the PMMA layer is estimated to be >4%; the local strain at the microbar region could be much higher and above the tensile limit,[33] which induced film rupture that also broke the attached nanowire (Supplementary Fig. 4). Replacing the PMMA carrier layer with other candidates of increased stretchability is expected to yield broader range in assembly height.

Adding microbars in each assembly site is expected to yield longer spanning in the structure (Fig. 1(vi)). Fig. 3i shows a Si nanobridge, in which the nanowire is supported by an array of four microbars (2.1 µm high, 6 µm pitch) covering a length >25 µm. As empirical results show that a microbar of 2.1 µm height yields a suspending arm ~4 µm (Fig. 3e), it is expected that a pitch <8 µm can yield full suspension in the nanowire, whereas a pitch >8 µm can yield damped nanowire (Supplementary Fig. 5). Likewise, the configuration of nanowire suspension is largely determined by the mechanical property of the carrier layer; increasing the mechanical rigidity in the carrier layer is expected to yield larger suspension. The transfer-enabled assembly (Fig. 1) also indicates that multiple transfers can be employed to create hierarchical multiwire structures. We demonstrated this concept in Fig. 3j, in which a second orthogonal nanowire transfer produced the

nanoscale frame of a nanotent. Multiple transfers, combined with structural engineering in the microbars, are expected to yield advanced hierarchical nanowire 3D structures.

We further exploited the 3D nanowire structures for device application. Si nanowires, due to the nanoscale confinement, were revealed to have a giant *piezoresistance* effect[34] featuring a greatly enhanced gauge factor compared to many other materials.[35] As *piezoresistance* effect is commonly employed in various mechanical sensors,[36-38] Si nanowires can be used to make ultrasensitive mechanical nanosensors. However, previous planar Si nanowire devices, due to a strong mechanical coupling to the substrate, can only detect global strain >1% (*e.g.*, substrate bending).[39] 3D structural engineering at nanoscale can effectively improve mechanical sensitivity.[38] Here the 3D structure effectively decouples the nanowire from the substrate, leading to the possibility of sensing local strain at much smaller scale.

Proof-of-concept devices were fabricated by patterning the suspended nanowire with a pair of metal electrodes and embedding the device in a PDMS elastomer (Fig. 4a). Mechanical pressure was vertically applied to the PDMS substrate. The nanowire device showed increased conductance G with the increase in applied pressure P (Fig. 4b, inset). Statistics from different devices yielded consistent responses (Fig. 4b), yielding an average sensitivity $(\Delta G/G)/\mathrm{P} \sim (5.0\pm0.76)\times10^{-5}\ \mathrm{kP}^{-1}$. Computer simulation was employed to study the local strain the nanowire experienced, which showed a net compressive one linearly increasing with the increase in applied pressure (Fig. 4c). The estimated average *pieozoresistance* coefficient, defined as the relative change in conductivity per unit stress, was $-(490\pm75)\times10^{-11}\ \mathrm{Pa}^{-1}$ (Methods) that was considerably larger than the typical values (-17 to $-94\times10^{-11}\ \mathrm{Pa}^{-1}$) in bulk Si.[34] The corresponding average gauge factor, defined as relative resistance change per unit strain, was ~920 ± 140 (Methods) that is more than an order of magnitude larger than typical values in many materials.[35] Both values are consistent to reported enhanced values in Si nanowires.[34] At the pressure of 4 kPa, the equivalent force exerted along the nanowire axis was estimated to be ~29 pN (Methods). This force is orders of magnitude lower than typical detection limit in other mechanical sensors,[36,37] showing that the 3D nanowire sensor has the great potential to serve as a nanoscale probe for ultrasensitive force detection. Note that at a global scale (*e.g.*, for pressure detection), the mechanical transduction is largely limited by the encapsulating elastomer (PDMS). A softer elastomer with decreased mechanical modulus is expected to improve mechanical transduction (*i.e.*, increased deformation at the nanowire region) and hence enhance the pressure sensitivity. This was experimentally verified. For example, a softer

PDMS elastomer (elastic modulus ~0.15 MPa) correspondingly improved the detection limit to 0.8 kPa (Fig. 4, inset) and doubled the pressure sensitivity to $(\Delta G/G)/P \sim (12.3\pm1.3)\times10^{-5}$ kP^{-1} (Fig. 4d). Such trend also indicates that by designing effective mechanical transduction,[41] ultrasensitive pressure sensors may be also realized by using the 3D nanowire structures.

In summary, we have shown the assembly of 3D suspended nanowire arrays in a controllable way. Modulating the mechanical property in the carrier layer and the substrate geometry are expected to yield diverse 3D nanowire structures. The added geometric freedom in assembled nanowires can lead to new device concepts and functions, which was preliminarily demonstrated in the construction of a localized force probe achieving high sensitivity. The concept and methodology can be employed in other low-dimensional nanomaterials to yield broad 3D nanostructures and devices.

References

1. Lieber, C.M. *MRS Bull*. **2011**, 36, 1052-1063.
2. Lu, W.; Lieber, C. M. *Nat. Mater*. **2007**, 6, 841–850.
3. Zhang, A.; Zheng, G.; Lieber, C.M. Nanowires: Building blocks for nanoscience and nanotechnology, Springer 2016.
4. Wang, M. C. P.; Gates, B. D. *Mater. Today* **2009**, 12, 34–43.
5. Yu, G.; Lieber, C.M. *Pure Appl. Chem*. **2010**, 82, 2295-2314.
6. Yan, H.; Choe, H.S.; Nam, S.W.; Hu, Y.; Das, S.; Klemic, J.F.; Ellenbogen, J.C.; Lieber, C.M. *Nature* **2011**, 470, 240-244.
7. Li, M.; Bhiladvala, R. B.; Morrow, T. J.; Sioss, J. A.; Lew, K.-K.; Redwing, J. M.; Keating, C. D.; Mayer, T. S. *Nat. Nanotech*. **2008**, 3, 88–92.
8. Freer, E. M.; Grachev, O.; Duan, X.; Martin, S.; Stumbo, D. P. *Nat. Nanotech*. **2010** 5, 525–530.
9. Yao, J.; Yan, H.; Lieber, C.M. *Nat. Nanotechnol*. **2013**, 8, 329-335.
10. Yao, J.; Yan, H.; Das, S.; Klemic, J.; Ellenbogen J.; Lieber, C.M. *Proc. Natl. Acad. Sci. USA* **2014**, 111, 2431-2435.
11. Shim, W.; Yao J.; Lieber, C.M. *Nano Lett*. **2014**, 14, 5430-5436.
12. Zhang, A.; Lieber, C.M. *Chem. Rev.* **2016,** 116, 215-257.

13. Tian, B.; Lieber, C.M. *Chem. Rev*. DOI: 10.1021/ACS.CHEMREV.8B00795, 17 APRIL 2019.
14. Jiang, Y. W.; Tian, B. Z. *Nat. Rev. Mater*. **2018**, 3, 473-490.
15. Tian, B.; Liu, J.; Dvir, T.; Jin, L.; Tsui, J.H.; Qing, Q.; Suo, Z.; Langer, R.; Kohane D.S.; Lieber, C.M. *Nat. Mater*. **2012**, 11, 986-994.
16. Dai, X.; Zhou, W.; Gao, T.; Liu, J.; Lieber, C.M. *Nat. Nanotechnol*. **2016**, 11, 776-782.
17. Schuhmann, T.G.; Yao, J.; Hong, G.; Fu T.-M.; Lieber, C.M. *Nano Lett*. **2017**, 17, 5836−5842.
18. Service, R. F. *Science* **2013**, 340, 1162-1165.
19. Dai, X.; Hong, G.; Gao T.; Lieber, C.M. *Acc. Chem. Res*. **2018**, 51, 309−318.
20. Yang, X.; Zhou, T.; Zwang, T.J.; Hong, G.; Zhao, Y.; Viveros, R.D.; Fu, T.-M.; Gao, T.; Lieber, C.M. *Nat. Mater*. **2019**, 18, 510–517.
21. Tian, B.; Cohen-Karni, T.; Qing, Q.; Duan, X.; Xie, P.; Lieber, C.M. *Science* **2010**, 329, 831-834.
22. Duan, X.; Gao, R.; Xie, P.; Cohen-Karni, T.; Qing, Q.; Choe, H.S.; Tian, B.; Jiang, X.; Lieber, C.M. *Nat. Nanotechnol*. **2012**, 7, 174-179.
23. Qing, Q.; Jiang, Z.; Xu, L.; Gao, R.; Mai, L.; Lieber, C.M. *Nat. Nanotechnol.* **2014**, 9, 142-147.
24. Zhao, Y.; Yao, J.; Xu, L.; Mankin, M.; Zhu, Y.; Wu, H.; Mai, L.; Zhang, Q.; Lieber, C.M. *Nano Lett*. **2016**, 16, 2644-2650.
25. Khang, D. Y.; Jiang, H.; Huang, Y.; Rogers, J.A. *Science* **2006**, 311, 208-212.
26. Xu, S; Yan, Z.; Jang, K.; Huang, W.; Fu, H.; Kim, J.; Wei, Z.; Flavin, M.; McCracken, J.; Wang, R.; Badea, A.; Liu, Y.; Xiao, D.; Zhou, G.; Lee, J.; Chung, H. U.; Cheng, H.; Ren, W.; Banks, A.; Li, X.; Paik, U.; Nuzzo, R. G.; Huang, Y.; Zhang, Y.; Rogers, J. A. *Science* **2015**, 347, 154-159.
27. Ling, Y.; Zhuang, X.; Xu, Z.; Xie, Y.; Zhu, X.; Xu, Y.; Sun, B.; Lin, J.; Zhang, Y.; Yan. Z. *ACS nano* **2018**, 12, 12456-12463.
28. Ryu. S. Y.; Xiao, J.; Park, W.; Son, K. S.; Huang, Y.; Paik, U.; Rogers, J. A. *Nano Lett.* **2009**, 9, 3214-3219.
29. Xu, F.; Lu, W.; Zhu, Y. *ACS Nano*, **2011**, 5, 672–678.
30. Li, H.; Wu, J.; Huang, X.; Yin, Z.; Liu, J.; Zhang, H. *ACS Nano*, **2014**, 8, 6563–6570.

31. Fan, Z.; Ho, J. C.; Jacobson, Z. A.; Yerushalmi, R.; Alley, R. L.; Razavi, H.; Javey, A. *Nano Lett*. **2008**, 8, 20–25.
32. Reserbat-Plantey, A.; Kalita, D.; Han, Z.; Ferlazzo, L.; Autier-Laurent, S.; Komatsu, K.; Li, C.; Weil, R.; Ralko, A.; Marty, L.; Gueron, S.; Bendiab, N.; Bouchiat, H.; Bouchiat, V. *Nano Lett*. **2014**, 14, 5044–5051.
33. Richeton, J.; Ahzi, S.; Vecchio, K.S.; Jiang, F.C.; Adharapurapu, R.R. *Int. J. Solids Struct*. **2006**, 43, 2318–2335.
34. He, R.; Yang, P. *Nat. Nanotechnol*. **2006**, 1, 42-46.
35. Hrovat, M.; Belavic, D.; Samardzija, Z.; Holc, J. *J. Mater. Sci*. **2011**, 36, 2679-2689.
36. Hammock, M. L.; Chortos, A.; Tee, B. C.-K.; Tok, J. B.-H.; Bao, Z. *Adv. Mater*. **2013**, 25, 5997–6038.
37. Chortos, A.; Liu, J.; Bao, Z. *Nat. Mater*. **2016**, 15, 937-950.
38. Yin, B.; Liu, X.; Gao, H.; Fu, T.; Yao, J. *Nat. Commun*. **2018**, 9, 5161.
39. Liu, J.; Xie, C.; Dai, X.; Jin, L.; Zhou, W.; Lieber, C.M. *Proc. Natl. Acad. Sci. USA* **2013**, 110, 6694-6699.
40. Mannsfeld, S.C.B.; Tee, B.C.K.; Stoltenberg, R.M.; Chen, C.V.H.H.; Barman, S.; Muir, B.V.O.; Sokolov, A. N.; Reese, C.; Bao, Z. *Nat. Mater*. **2010**, 9, 859-864.

Notes. The authors declare no competing financial interest.

Acknowledgement. J.Y. acknowledges the support of this work by a National Science Foundation (NSF) Award CBET-1844904 and the generous material support from Prof. Charles Lieber at Harvard University. J.Y. also acknowledges the help in material (elastomer) preparation from Christopher Barney and Prof. Alfred J. Crosby in the Polymer Science and Engineering Department and the equipment (optical stage) share from Prof. Tingyi Liu in the Mechanical and Industrial Engineering Department. Part of the device fabrication work was conducted in the clean room of the Center for Hierarchical Manufacturing (CHM), an NSF Nanoscale Science and Engineering Center (NSEC) located at the University of Massachusetts Amherst.

Supporting Information. The Supporting Information is available free of charge on the ACS Publications website:

Materials and Methods, nanowire peel-off process (Figure S1), optical images of assembled nanowires (Figure S2), aligned transfer process (Figure S3), optical images of transferring nanowires onto high (*e.g.*, > 4 μm) microbars (Figure S4), SEM image of assembled nanowire structure over three microbars that were 10 μm spaced (Figure S5), and supplementary references.

Figure Legends

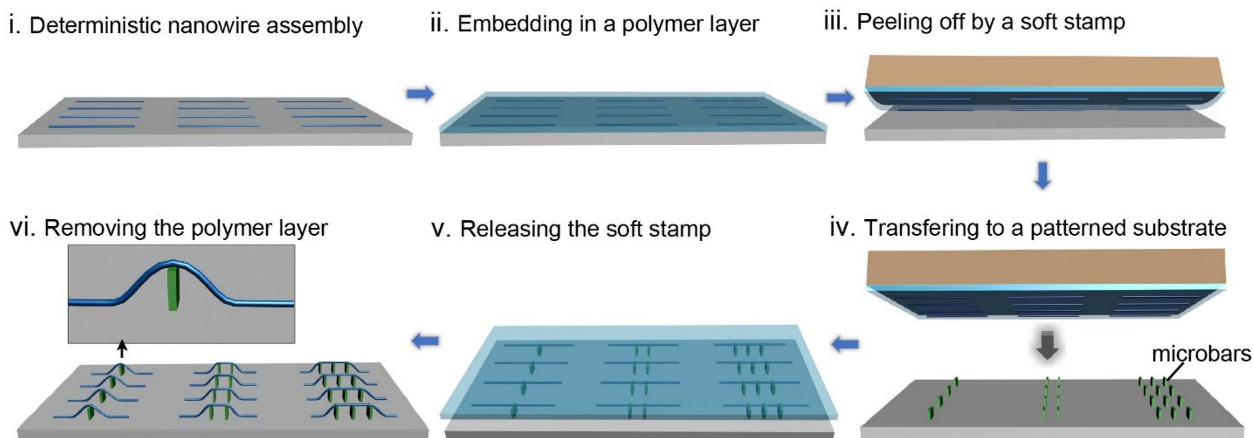

Figure 1. Schematics of the proposed scheme of constructing 3D nanowire suspended structures.

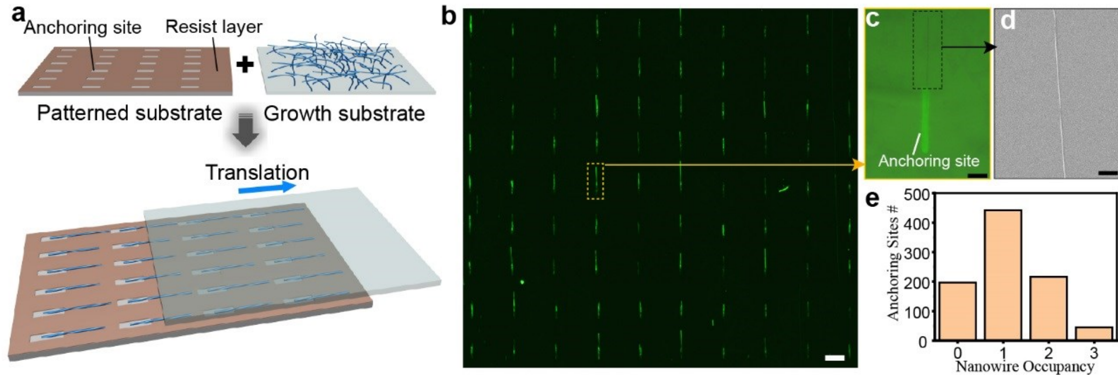

Figure 2. **a**, Schematics of deterministic assembly of planar nanowires by a 'combing' strategy. **b**, Dark-field optical image of an assembled 10×10 matrix. Scale bar, 50 µm. **c**, Zoom-in bright-field image of an assembled site, with the light window indicating the exposed SiO_2 surface (anchoring site). Scale bar, 4 µm. **d**, SEM image of the extending nanowire part on the resist. Scale bar, 1 µm. **e**, Distribution of the number of nanowires in 900 assembled sites.

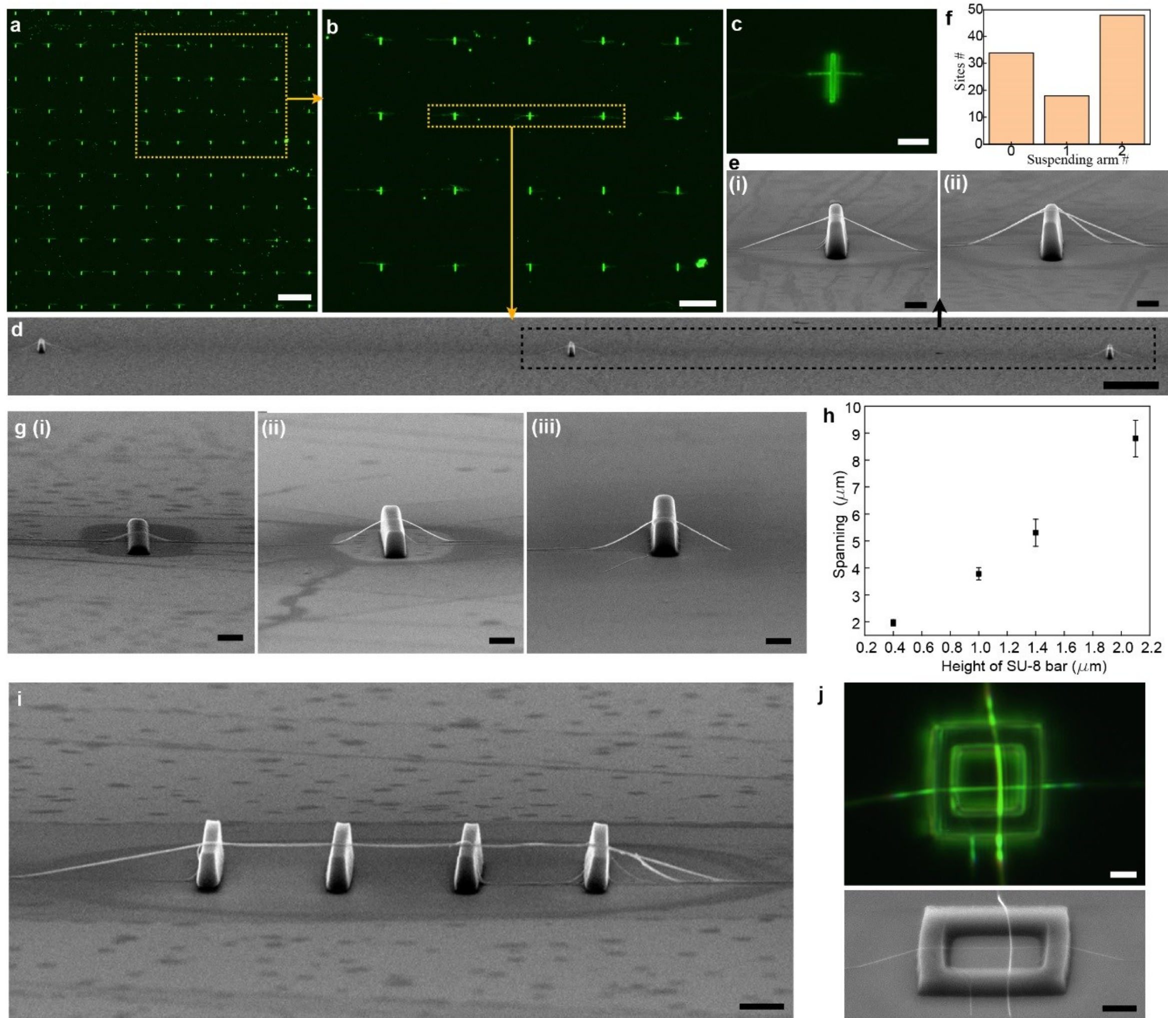

Figure 3. **a**, Dark-field optical image of an assembled 10×10 matrix. Scale bar, 100 μm. **b**, Zoom-in image of 5×4 matrix, showing (transverse) nanowires crossing over the (perpendicular) SU-8 microbars. Scale bar, 50 μm. **c**, Zoom-in image of one assembled nanowire structure. Scale bar, 3 μm. **d**, SEM image of an array of three assembled nanowire structures. Scale bar, 10 μm. **e**, Zoom-in SEM images of two representative 3D nanowire structures. Scale bar, 1 μm. **f**, Distribution of assembled sites with no nanowire (0), half-suspending nanowire (1), and full-suspending nanowire (2) from the 100 assembled sites. **g**, Representative SEM images of assembled 3D nanowire structures with (i) 0.4, (ii) 1, and (iii) 1.4 μm heights in the microbars. Scale bar, 1 μm. **h**, The average nanowire spanning *v.s.* the height of the microbar. **i**, SEM image of a nanowire spanning across an array of four microbars. Scale bar, 2 μm. **j**. Dark-field optical image (top) and SEM image (bottom) of crossed nanowire suspensions. Scale bars, 2 μm.

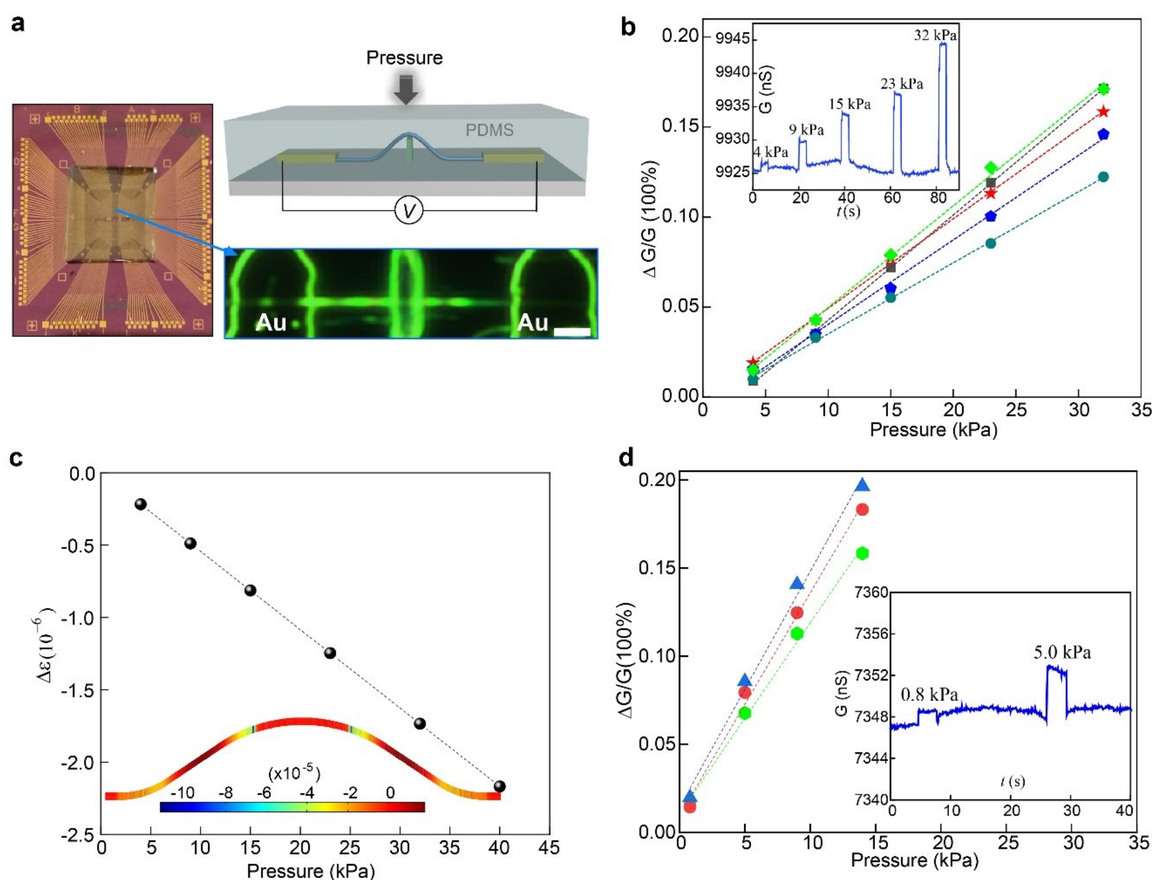

Figure 4. **a**, (Top right) Schematic of a 3D 'convex' nanowire device embedded in a PDMS elastomer, with vertical pressure applied to the PDMS top surface and the conductance in the device simultaneously monitored. (Left) Optical image of an integrated 3D nanowire device chip, with a thin layer of PDMS cured on top and encapsulating the devices. (Bottom right) Zoom-in dark-field image of the 3D nanowire device with electric contacts (Au) defined. Scale bar, 2 µm. **b**, Relative conductance change (ΔG/G) in the nanowire devices (*N*=5) with respect to applied pressure. (Inset) A representative current change (V_{ds}=1 V) at different pressures. **c**, Induced net tensile strain change (Δε) along the nanowire axis at different applied pressure, revealed by computational mechanical simulation. The bottom inset shows the local tensile strain distribution across the nanowire structure. **d**, Relative conductance change (ΔG/G) with respect to different applied pressure from a nanowire device embedded in a softer PDMS layer (elastic modulus ~0.15 MPa). (Inset) A representative current change (V_{ds}=1 V) at different pressures.

For Table and Contents only.